Applied Mathematical Modelling 40 (2016) 2002–2014

Contents lists available at ScienceDirect

Applied Mathematical Modelling

journal homepage: www.elsevier.com/locate/apm

A new direct design method of wind turbine airfoils and wind tunnel experiment

Jin Chen [a,*], Quan Wang [a,b,*], Shiqiang Zhang [a,c], Peter Eecen [c], Francesco Grasso [c]

[a] State Key Laboratory of Mechanic Transmission, Chongqing University, Chongqing 400030, China
[b] School of Mechanical Engineering, Hubei University of Technology, Wuhan 430068, China
[c] Energy Research Centre of the Netherlands, Petten 1755ZG, The Netherlands

ARTICLE INFO

Article history:
Received 17 December 2012
Revised 17 March 2015
Accepted 22 September 2015
Available online 8 October 2015

Keywords:
Wind turbine airfoil
Shape function
Optimisation design
Aerodynamic performance
Wind tunnel experiment

ABSTRACT

A general parametric representation function (Shape Function) for wind turbine – dedicated airfoils based on Taylor high-order polynomial series is presented for the first time. The design space and shape control function of the airfoil have been studied. The objective of the high-performance WT (Wind Turbine) airfoils was to maximise the lift/drag ratio at the design angle of attack both in free and fixed transitions. The optimised mathematical model of the airfoils is built combing genetic algorithm and the flow solver RFOIL. The new airfoil family (ranging in thickness from 15 to 20%) with target characteristics were designed for variable-speed operation with pitch control of large megawatt-sized rotors. Wind tunnel experiments for the WT180 airfoil were carried out for both clean and rough conditions. The experimental results for the lift and drag coefficients agree well with the RFOIL predictions. The testing verified the high lift/drag ratio and the high maximum lift coefficient for the WT180 airfoil. The results indicate that this novel design method is feasible to optimise wind turbine airfoils.

1. Introduction

It is necessary to accurately predict energy capture of wind turbines which is influenced by the aerodynamic design of wind turbine airfoils and blades. One important key element in the aerodynamic design of wind turbine blade is the use of special tailored airfoils to improve the ratio of energy capture and to reduce cost of energy. It is well known that the aerodynamic design of wind turbine blades is mainly concerned with the airfoil design. Hence, this paper focuses on the establishing of mathematic model and the design method of optimising wind turbine airfoils with high aerodynamic performances.

The development of wind turbine airfoils was, to some extent, built upon the aircraft airfoils, such as NACAXX, FX airfoils series, and so on. In the middle 1980's, Tangler and Somers designed nine airfoil families for several size rotors using Eppler Airfoil Design and Analysis Code called reverse design method [1–3]. DU airfoil families with the thickness from 15 to 40% were designed by wind energy research Institute of Delft University, associated with Energy research Centre of the Netherlands (ECN) and National Aerospace Laboratory of the Netherlands (NLR) using mixed inverse design method. The aerodynamic performance of DU airfoil families were calculated by RFOIL software [4]. It has been verified that the calculated results were agreed with the wind tunnel test data. The structural and geometrical compatibility and deep stall features were considered in the design process for DU airfoil series. And the best performing airfoils can be recognised by a restricted upper-surface thickness and an S-shape lower surface for aft-loading [5–6]. Compared with traditional airfoils, the DU airfoil families exhibited better aerodynamic characteristics. From the middle 1990's, the four airfoil families (RISØ-A1, RISØ-P, RISØ-B1 and RISØ-C1) were designed

* Corresponding authors. Tel.: +86 2365102412.
E-mail addresses: chenjin413@cqu.edu.cn (J. Chen), quan_wang2003@163.com (Q. Wang).

http://dx.doi.org/10.1016/j.apm.2015.09.051
S0307-904X(15)00585-5/

Nomenclature

a	Geometrical scale factor
C_L, C_D	Lift and drag coefficients
C_P	Pressure distribution coefficient
c	Chord (m)
$L_{\max}$	The location of the maximum thickness
Ma	Mach number
Re	Reynolds number
th	Airfoil thickness-to-chord ratio
ρ	Airfoil shape function
ζ	Plane of airfoil
z'	Plane of circle curve

Greek letters

α	Angle of attack (degrees)
ε, Δ	X-axis offset of the near circle; y-axis offset of the near circle
λ_1, λ_2	Weight coefficient

by RISØ National Laboratory in Denmark [7]. These airfoils adapted to different power sizes, operating conditions and control modes for wind turbines. By increasing the thickness and chord length ratio of the airfoil, they could not only reduce the weight and fatigue load of wind turbines but also improve annual energy production of wind turbines [8]. And more importantly, a direct design method for wind turbine airfoils based on numerical optimisation, and the flow solver XFOIL [9] was initiated in their work. This method can handle the problems where interdisciplinary design objectives and multiple design points were involved. Most of the wind turbine airfoils were designed by using traditional inverse methods where the airfoil surface flow was prescribed at specified operational conditions, and a shape was achieved when it could generate these surface conditions. In addition, SOBIECZKY [10] presented a method named PARSEC to design airfoils; and a modern airfoil was designed by controlling the airfoil geometry parameters. HÁJEK [11] presented an improved PARSEC method to design airfoils, and a brand new airfoil was optimised. With the development of wind turbine airfoils, Bjork, Soemarwoto, Habali, Nielsen, Baker, Bermudez and A.F.P.Ribeiro [12–18] have also made other significant contributions to this field. Those new wind turbine airfoils not only improved the efficiency of wind energy, but were also adapted to different operating conditions. Recently, Shen, Chen presented a general integral equation of airfoil profiles based on generalised function and Trajkovski conformal transform theory. A graph which is similar to a circle can be changed into a wind turbine airfoil by using the proposed method. Furthermore, the airfoil profiles can be controlled by changing the coefficients of the trigonometric series [19]. However, it is hard to control the changing coefficients when the wind turbine airfoil is designed, and also there is lack of the validation of the wind tunnel experiments. Therefore, it is necessary to present a novel mathematic modelling with other form of shape function expression to optimise wind turbine airfoils efficiently. And the airfoil designed need to be verified through experiment.

In this paper, a novel direct design method for the wind turbine airfoils is introduced based on a general parametric representation function (Shape Function) for wind turbine airfoils. A high-order Taylor series is proposed to represent Shape Function. The design space and shape control function of airfoils are studied in detail. The optimised mathematic model of the wind turbine airfoil is built combing the genetic algorithm and the flow solver RFOIL. By controlling the coefficients of the Shape Function, three airfoils (named WT airfoils families) with high aerodynamic performance are designed. Lastly, the aerodynamic performance of the WT180 airfoil is verified by wind tunnel test.

2. Design methods

The traditional methods for inverse design have been applied to the designs of most wind turbine airfoils, and the current method is a direct method which combines numerical optimisation with the flow solver RFOIL [5–6]. The airfoil shape is acquired through a number of design variables from the optimisation controlled by design objectives and constraints. Direct methods are generally interdisciplinary and multi-point, and integrated response parameters, such as airfoil lift and drag, can be directly used as design objectives when applying direct method. Moreover, boundary layer response parameters, such as skin friction and transition point location, can be constrained or used as objectives.

2.1. Shape function

A conformal transformation consists in mapping a region of one plane on another plane in such a manner that the detailed shape of infinitesimal elements of area is not changed. A circle can be transformed into a shape resembling that of a blade section by Joukowsky transform [20].

The coordinates of z' are defined by the relation of $z' = a \times e^{\varphi + i\theta}$ in reference 20 page 54. In this paper, the shape function $\rho(\theta)$ is defined by the relation of $\rho(\theta) = e^{\varphi}$ which is the function of θ. Then, a universal function of the coordinates of z' is as

follow:

$$z' = a \times \rho(\theta) \times e^{i\theta} \tag{1}$$

Substitution of Eq. (1) into the equation $\varsigma = z' + a^2/z'$ which is found in reference 20 page 54,

$$\varsigma = a(\rho e^{i\theta} + \rho^{-1} e^{-i\theta}) \tag{2}$$

According to Euler's formula, the Formula (2) is transformed into the Cartesian coordinate system:

$$\begin{cases} x = a\left(\rho + \frac{1}{\rho}\right)\cos(\theta) \\ y = a\left(\rho - \frac{1}{\rho}\right)\sin(\theta) \end{cases} \tag{3}$$

Based on the Taylor series expansion concept, any function can be expanded into a Taylor series using a high-order polynomial; therefore, a high-order polynomial is firstly introduced to represent $\rho(\theta)$:

$$\rho(\theta) = C_0 + C_1\theta + C_2\theta^2 + C_3\theta^3 + \cdots C_k\theta^k + \cdots \tag{4}$$

Where $k = 0, 1, 2, \ldots n$; $C_0, C_1, C_2, \ldots C_k, \ldots$; and $\theta \in [0, 2\pi]$.

Eq. (4) is a general function that describes the unique shape of the geometry between the round nose and the sharp aft end. Here, the $\rho(\theta)$ is defined as the airfoil shape function. By changing the value of the coefficients of each order of the shape function $\rho(\theta)$, one can obtain various airfoils with different thicknesses, cambers, leading edge radius and trailing edge angles.

2.2. The control equation of the shape function

As it is known that the Formula (4) is the shape function of the airfoil profiles. In this section the characteristic of control equation of the shape function will be studied. And then, two examples are selected to verify the expression can describes the airfoil profiles.

In order to ensure that the mapped airfoil is closed and with a sharp trailing edge, the near circle on the z' plane should have a singularity point (which intersects the point $a + 0 \times i$).

Substituting the relevant values of θ into Eqs. (4) and (1)

$$\begin{cases} a \cdot \rho(0) = a \\ a \cdot \rho(2\pi) = a \end{cases} \tag{5}$$

The first control function is obtained:

$$\begin{cases} C_0 = 1 \\ 2\pi C_1 + 4\pi^2 C_2 + \cdots + 2^k \pi^k C_k + \cdots = 0 \end{cases} \tag{6}$$

The coordinates of the centre of the circle are variables, and the variation of them modifies the shape of the resulting airfoil. If the circle offsets on the x-axis, the circle maps in an airfoil that is symmetric with respect to the x-axis. Assuming that the circle passes through the point $((1+\varepsilon)a + 0 \times i)$, substituting the relevant values of θ into Eqs. (4) and (1)

$$a \cdot \rho(\pi) = a \cdot (1 + \varepsilon) \tag{7}$$

Here ε is a coefficient for offsetting on the x-axis.

The second control function takes the form:

$$C_0 + \pi C_1 + \pi^2 C_2 + \cdots + \pi^k C_k + \cdots = 1 + \varepsilon \tag{8}$$

To generate an asymmetric airfoil (cambered airfoil), the circle should also be offset on the y-axis. Assuming that the offset value on the y-axis is $\Delta \cdot a$, and substituting the relevant values of θ into Eqs. (4) and (1)

$$a \cdot \rho\left(\frac{\pi}{2}\right) = a \cdot \rho\left(\frac{3\pi}{2}\right) + \Delta \cdot a \tag{9}$$

Here Δ is a coefficient for offsetting on the y-axis.

Therefore, the third control function becomes:

$$C_0 + \frac{\pi}{2}C_1 + \frac{\pi^2}{4}C_2 + \cdots + \left(\frac{\pi}{2}\right)^k C_k + \cdots = C_0 + \frac{3\pi}{2}C_1 + \frac{9\pi^2}{4}C_2 + \cdots + \left(\frac{3\pi}{2}\right)^k C_k + \cdots + \Delta \tag{10}$$

To summarise, moving the centre of the circle along the x-axis gives thickness to the airfoil, moving the centre of the circle along the y-axis gives camber to the airfoil. The general control function of the airfoil is obtained by Eqs. (6), (8) and (10):

$$\begin{cases} C_0 = 1 \\ 2\pi C_1 + 4\pi^2 C_2 + \cdots + 2^k \pi^k C_k + \cdots = 0 \\ \pi C_1 + \pi^2 C_2 + \cdots + \pi^k C_k + \cdots = \varepsilon \\ \pi C_1 + 2\pi^2 C_2 + \cdots + \frac{(3^k - 1)\pi^k}{2^k} C_k + \cdots = -\Delta \end{cases} \tag{11}$$

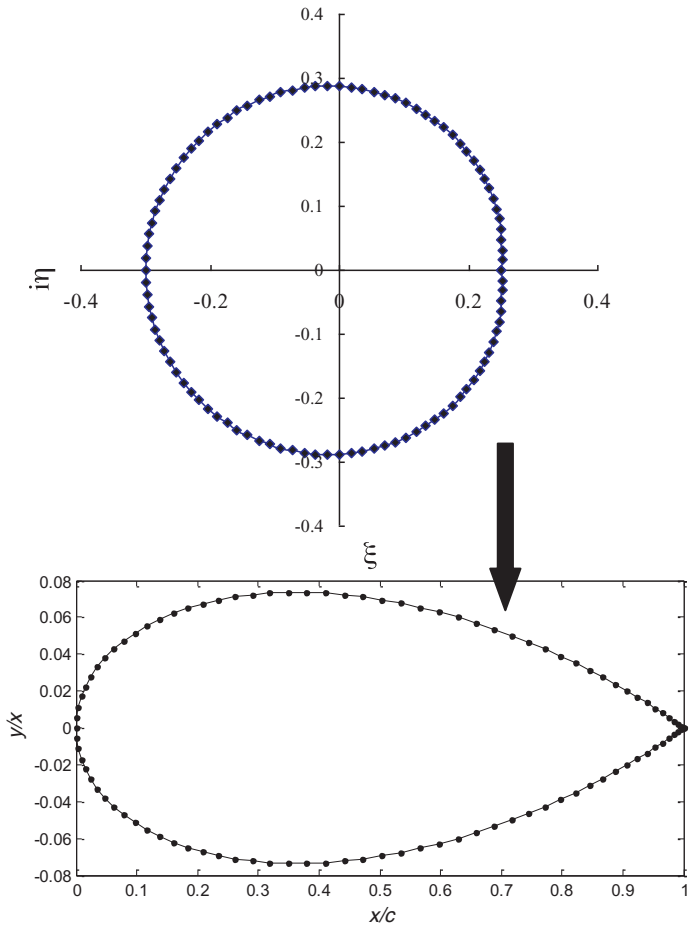

Fig. 1. The second order airfoil transformation.

Now, the two cases of second-order and third-order polynomial shape function are chosen to verify that the Eqs. (3) and (4) can represent the airfoil profiles.

Case 1. The Eq. (4) takes the form of a second-order polynomial:

$$\rho(\theta) = C_0 + C_1\theta + C_2\theta^2 \tag{12}$$

The coefficients of the Eq. (12) are given by Eq. (11):

$$C_0 = 1, \quad C_1 = \frac{2\varepsilon}{\pi}, \quad C_2 = -\frac{\varepsilon}{\pi^2}$$

Selecting $\varepsilon = 0.2$, and the coefficients C_1, C_2 can be obtained:

$$C_1 = \frac{2}{5\pi}, \quad C_2 = -\frac{1}{5\pi^2}$$

The coefficients C_1, C_2 are substituted into the shape function (12), and then the symmetry airfoil is plotted after conformal transformation (as shown in Fig. 1).

Case 2. The Eq. (4) takes the form of a third-order polynomial:

$$\rho(\theta) = C_0 + C_1\theta + C_2\theta^2 + C_3\theta^3 \tag{13}$$

The coefficients of the Eq. (13) are given by Eq. (11):

$$C_1 = \frac{16\Delta/3 + 4\varepsilon}{2\pi}, \quad C_2 = -\frac{\varepsilon + 4\Delta}{\pi^2}, \quad C_3 = \frac{4\Delta}{3\pi^3}$$

To illustrate that the airfoil exhits asymmetry characterastic, the coefficients Δ and ε must be known, supposing $\Delta = 0.2$, $\varepsilon = 0.15$, and the coefficients C_1, C_2 and C_3 can be obtained:

$$C_1 = \frac{5}{6\pi}, \quad C_2 = -\frac{19}{20\pi^2}, \quad C_3 = \frac{4}{15\pi^3}$$

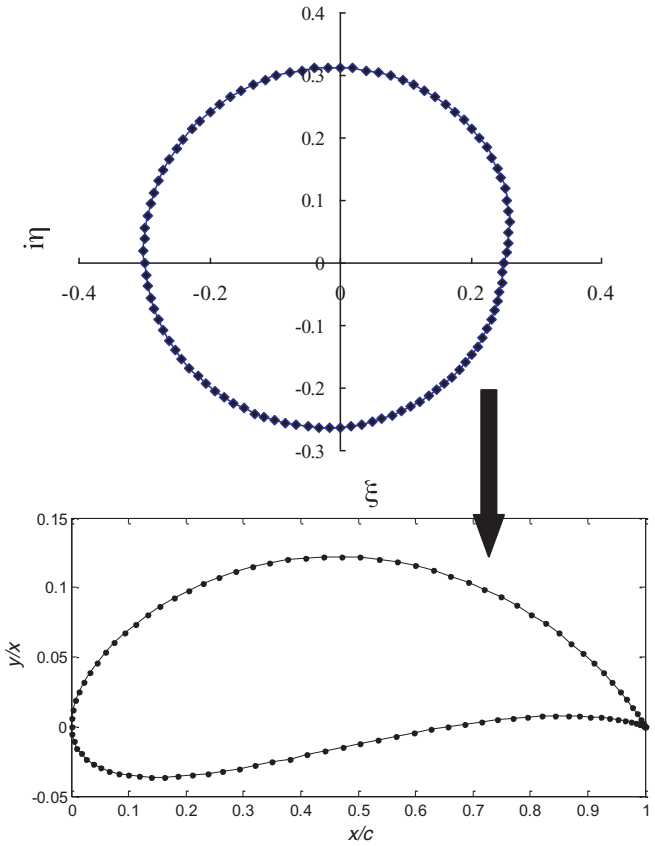

Fig. 2. The third order airfoil transformation.

The coefficients C_1, C_2 and C_3 are substituted into the shape function (13), and then the asymmetry airfoil is plotted after conformal transformation (as shown in Fig. 2).

From the above analysis, it is seen that a large number of airfoils can be generated from the shape function by adjusting the order and the values of the coefficients. Therefore, the coefficients of the airfoil shape function $\rho(\theta)$ are taken as design variables to optimise airfoils with high aerodynamic performance.

2.3. Design variables

Based on the general parametric representation function (Shape Function), select the second to ninth coefficients of airfoil shape function $\rho(\theta)$ as the design variable:

$$X = (C_1, C_2, C_3, C_4, C_5, C_6, C_7, C_8)^T \tag{14}$$

2.4. Objective function

To maximise the efficiency of the wind turbine, the main objective is to consider the aerodynamic performance of the airfoil. The first objective is to maximise the lift/drag ratio of the smooth working condition:

$$f_1(X) = \max\left(C_L/C_D\right)$$

where C_L and C_D are the lift and drag coefficients of the smooth condition, respectively, and the free transition model is used to simulate the smooth working condition.

The second objective is to maximise the lift-drag ratio of the roughness working condition:

$$f_2(X) = \max\left(C_L'/C_D'\right)$$

where C_L' and C_D' are the lift and drag coefficients of the roughness condition, respectively, and the fixed transition model is used to simulate the roughness working condition (the transition points for the suction and pressure sides were fixed to 1 and 10%, respectively).

Table 1
Rang of design variables.

	C_1	C_2	C_3	C_4	C_5	C_6	C_7	C_8
Max	0.2	0.2	0.1	0.6	0.1	0.1	0.1	0.01
Min	−0.2	−0.2	−0.2	0.1	−0.3	−0.1	−0.1	−0.01

The system objective is:

$$f(X) = \lambda_1 \cdot f_1(X) + \lambda_2 \cdot f_2(X) \tag{15}$$

where λ_1 and λ_2 are the weighting factor of two objectives, and $\lambda_1, \lambda_2 \in [0, 1]$, $\lambda_1 + \lambda_2 = 1$.

2.5. Design constraints

To conclude the definition of the optimisation problem, constraints are imposed on the design. To ensure the generated shape can totally cover the design space, upper and lower limits are imposed on the design variables:

$$X_{\min} \le X \le X_{\max} \tag{16}$$

The lower and upper values of each design parameters are shown in Table 1.

To generate the streamlined shape that looks like an airfoil, the coefficients of the shape function must satisfy the shape control function:

$$g_1(X) = C_0 - 1 = 0 \tag{17}$$

$$g_2(X) = \sum_{k=1}^{8} 2^k \pi^k C_k = 0 \tag{18}$$

$$g_3(X) = \sum_{k=1}^{8} \pi^k C_k - \varepsilon = 0 \tag{19}$$

$$g_4(X) = \sum_{k=0}^{8} \frac{(3^k - 1)\pi^k}{2^k} + \Delta = 0 \tag{20}$$

where ε and Δ are the horizontal coordinate offset and the longitudinal coordinate offset.

From the load viewpoint, a high design-C_L should be desired because this leads to smaller chords and, consequently, to lower storm loads.

$$g_5(X) = C_{L,d\,\min} - C_{L,d} \le 0 \tag{21}$$

New airfoils are designed by constraining the thickness-to-chord ratio between 15 and 20%. Also, the local shape of the airfoil and the location of the maximum thickness are of great importance. For the airfoils of a wind turbine, geometric compatibility is crucial. To ensure a smooth blade shape, the distinct airfoils for the different thicknesses need to match as a result of the variation in the thickness-to-chord ratio along the blade span. By constraining the location of the maximum thickness to between 25 and 32% of the chord, geometric compatibility was then ensured.

$$g_6(X) = th_{\min} - th \le 0 \tag{22}$$

$$g_7(X) = th - th_{\max} \le 0 \tag{23}$$

$$g_8(X) = L_1 - L_{\max} \le 0 \tag{24}$$

$$g_9(X) = L_{\max} - L_2 \le 0 \tag{25}$$

where th is the given maximum thickness, th_{min} is the minimum thickness for the designed airfoil, th_{max} is the maximum thickness for the designed airfoil, L_{max} is the location of the maximum thickness, L_1 equals to 0.25, and L_2 sets to 0.32.

Broadband trailing edge noise, which is generated by the passage of turbulent flow over the trailing edge, is perceived as the dominant noise from wind turbines. This type of noise relates to the airfoil free stream velocity and to the thickness and shape of the boundary layer at the trailing edge [7]. To prevent excessive boundary layer noise, the airfoil should have a sharp trailing edge.

$$y_{u,0.99} - y_{l,0.99} \le 0.01 \tag{26}$$

where $y_{u,\,0.99}$ and $y_{l,\,0.99}$ are the ordinate values of the upper surface and the lower surface at $x = 0.99$.

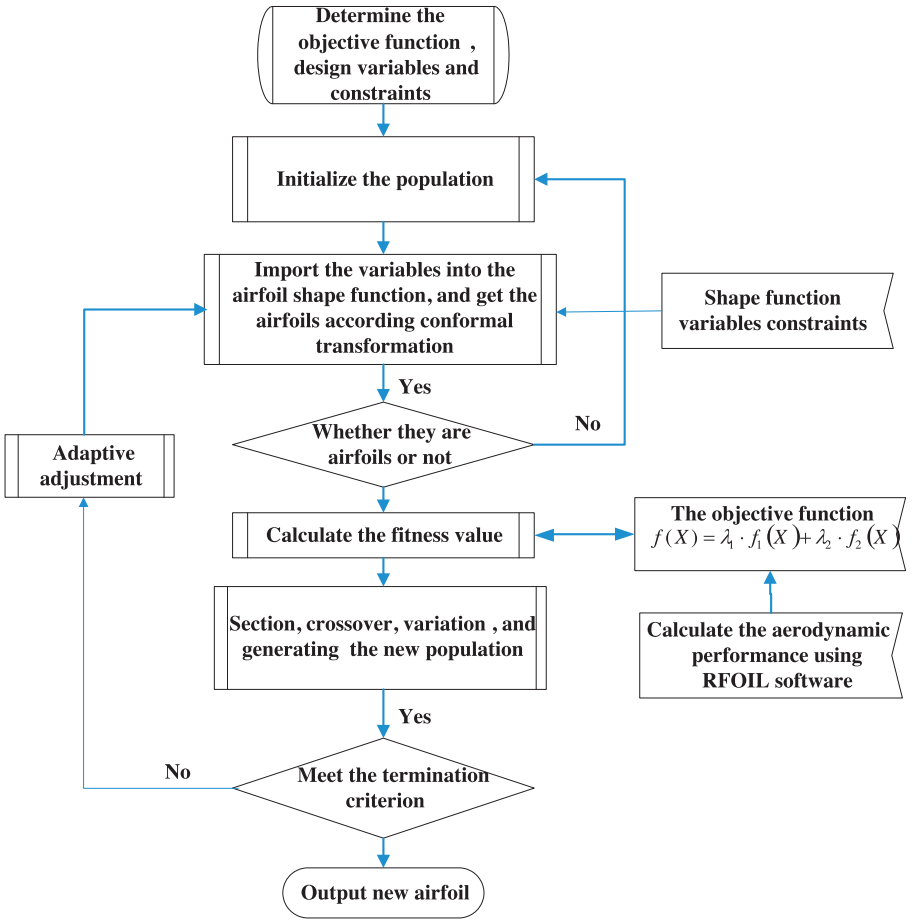

Fig. 3. GA algorithm flow chart of the airfoil optimisation.

2.6. Design algorithm

The combination of numerical optimisation and flow solver RFOIL software are shown in Fig. 3. A global method involving Genetic Algorithms is chosen to perform the optimisation. The GA method is less sensitive to local minima. The GA parameters are as follows: the population size is 30, the maximum generation number is 200, the crossover probability is 0.01 and the mutation probability is 0.7.

A bestpoke optimal code with GA is used to design the wind turbine airfoil. When the maximum number of generations was reached is the termination condition. The population is the design variables. The lower and upper values of each design variables are shown in Table 1. The population is initialised by random distribution in the range of the design variables. A special code is written to deal with the relationship between the objective function and the geometry parameters (such as the thickness, the location of its maximum, the camber and so on). Once the geometry parameters are not in a given reasonable range (the thickness is set 15 to 21%, the location of its maximum is 0.25 to 0.32, and the camber is set 0.01 to 0.04), the objective function will be multiplied by a penalty function.

3. Design results

The design is based on Reynolds and Mach numbers representative of a 2 MW wind turbine. Three high-performance airfoils (WT series) have been developed with a thickness-to-chord range from 15 to 20%.

Focusing on the conditions and requirements of most wind farms, the WT series airfoils were developed (High C_L/C_D, High C_L, and Insensitive). The characteristics of the WT series airfoils involve a trade-off between the aerodynamic performance of free transitions and fixed transitions. The weight coefficients for free transitions and fixed transitions are $\lambda_1 \in [0.4, 0.6]$ and $\lambda_2 = 1 - \lambda_1$, respectively. From these coefficients, the system level objective, $f(X) = \lambda_1 \cdot f_1(X) + \lambda_2 \cdot f_2(X)$, is established. The optimised results of the coefficients for the airfoil shape functions are shown in Table 2. Three WT airfoils (WT150, WT180 and WT201) were designed with a thickness range from 15 to 20%, where WT means Wind Turbine airfoil and the value after that represents 1/1000 of the airfoil thickness. Fig. 4 shows the shapes of the WT series airfoil.

Table 2
Coefficients of the airfoil shape functions.

Airfoil name	C_1	C_2	C_3	C_4	C_5	C_6	C_7	C_8
WT150	0.131796	−0.060058	−0.150282	0.154312	0.0149111	−0.066557	−0.00167887	7.47892e−005
WT180	0.135179	0.169777	−0.650805	0.526446	−0.199565	0.0399258	−0.00407183	0.000166823
WT201	0.136947	0.168366	−0.680133	0.555068	−0.210776	0.0421114	−0.00428201	0.000174758

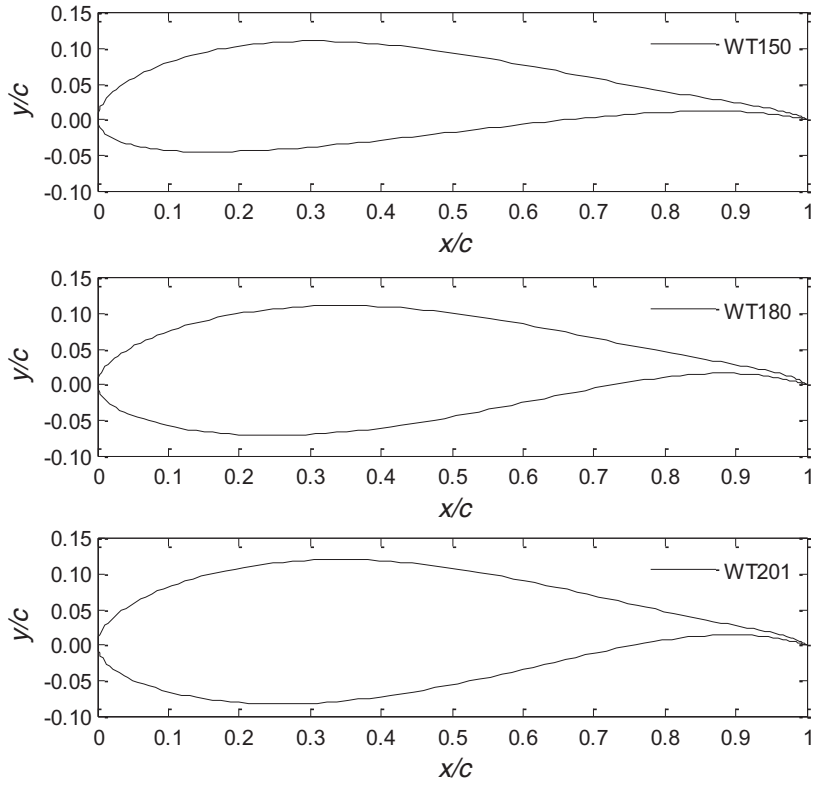

Fig. 4. The WT airfoil families shapes.

The maximum thickness of the WT180 airfoil is $th = 0.179998$, and the location of the maximum thickness is 0.294 chords from the leading edge ($L_{\max} = 0.294$). The maximum camber of the WT180 airfoil is $cam/c = 0.030005$ at $x/c = 0.4688$. To prevent excessive boundary layer noise, the airfoil has a sharp trailing edge.

To demonstrate the aerodynamic performance of the designed airfoils, a comparison is made between the new WT180 airfoil and some existing wind turbine airfoils. The aerodynamic results calculated by RFOIL agreed well with the experimental data [6], therefore, the results of the aerodynamic performance for the following airfoils in this section are also calculated from RFOIL. Figs. 5 and 6 show the aerodynamic performance comparisons between the new airfoils and commonly used wind turbine airfoils (NACA-63-418, S810) for the same working conditions ($\mathrm{Re} = 3.0 \times 10^6$, $\mathrm{Ma} = 0.2$). The maximum lift/drag ratio of the new airfoils is up to 151.556 for the working condition of a smooth surface; this maximum value appeared at the angle of attack $\alpha = 4.5^\circ$. For the rough surface condition, the maximum lift/drag ratio of the new airfoil is 91.4793 at the angle of attack $\alpha = 6.5^\circ$. The new airfoil is insensitive to the leading edge roughness condition and has good stall characteristics. In the main angle of attack, the new airfoils show a higher lift and lift/drag ratio than commonly used wind turbine airfoils for both working conditions of free and fixed transitions.

Table 3 shows the main aerodynamic parameters of the NACA-63-418, S810 and WT180 airfoils. Compared with the NACA-63-418 airfoil, the maximum C_L/C_D of the new WT180 airfoil increased 8 and 18.2% for the working conditions of free transition and fixed transition, respectively. Compared with the S810 airfoil, the maximum C_L/C_D of the new WT180 airfoil increased 19.6 and 50.2% for the working conditions of free transition and fixed transition, respectively.

On the whole, the newly designed WT180 airfoil was found to have much better on-design and off-design operational condition characteristics, and it showed a higher lift coefficient and a larger lift/drag ratio in both free transition and fixed transition conditions for the main working angle of attack. The results show that the new method is feasible for designing wind turbine airfoils.

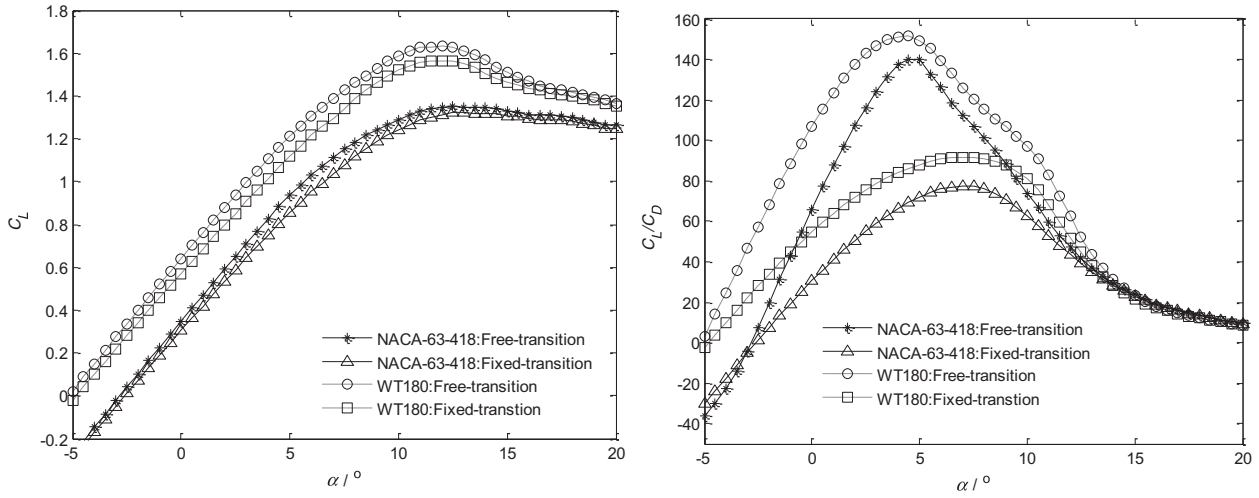

Fig. 5. Aerodynamic performances of the WT180 airfoil and the NACA-63-418 airfoil.

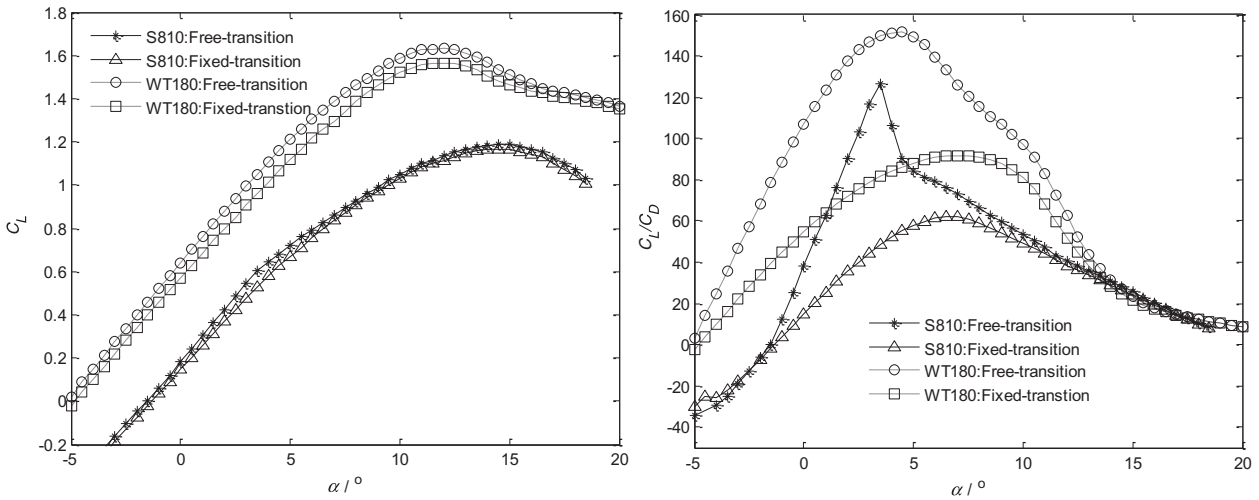

Fig. 6. Aerodynamic performances of the WT180 airfoils and the S810 airfoil.

Table 3
The main aerodynamic parameters of the airfoils (Re = 3.0×10^6, Ma = 0.2).

Airfoil name	Free transition		Fixed transition Xtrs = 0.01; Xtrp = 0.1	
	$C_{L\text{-}max}$	C_L/C_D-max	$C_{L\text{-}max}$	C_L/C_D-max
NACA-63-418	1.3521	140.302	1.3211	77.3897
S810	1.1871	126.674	1.1736	60.9084
WT180	1.6341	151.556	1.5647	91.4793

Table 4
Summary of the airfoil parameters (Re = 3.0×10^6, Ma = 0.2).

Airfoil name	Free-transition		Fixed –transition Xtrs = 0.01; Xtrp = 0.1		Max thickness	at x=	Max camber	at x=
	$C_{L\max}$	$(C_L/C_D)_{\max}$	$C_{L\max}$	$(C_L/C_D)_{\max}$				
WT150	1.7748	158.079	1.6504	97.6994	0.15059	0.254	0.037385	0.443
WT180	1.6341	151.556	1.5647	91.4793	0.179998	0.294	0.030005	0.688
WT201	1.5689	152.650	1.4211	83.0673	0.201031	0.305	0.028847	0.691

(a) Free transition (b) Fixed transition

Fig. 7. The wind tunnel test section with a test stand and a wake rake downstream of the airfoil section.

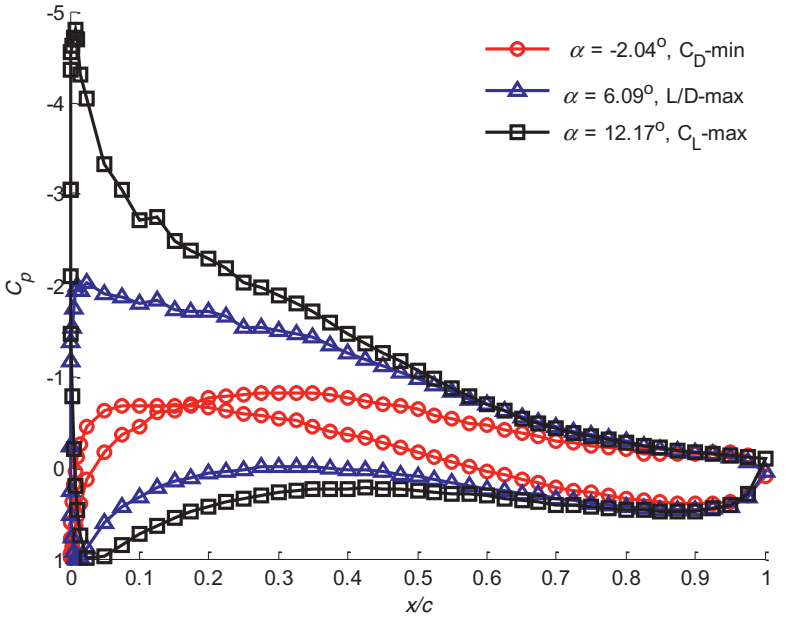

Fig. 8. The experimental pressure coefficient distribution at Re = 3.0×10^6.

In Table 4, the aerodynamic performances of WT series airfoils with thicknesses ranging from 15 to 20% are shown. The primary design driver was a high lift-to-drag ratio both in smooth and rough working conditions. For the free transition working condition, the maximum lift ranges from 1.5689 to 1.7748, and the maximum lift/drag ratio ranges from 152.650 to 158.079. For the fixed transition, the maximum lift ranges from 1.4211 to 1.6504, and the maximum lift/drag ratio ranges from 83.0673 to 97.6994.

4. Wind tunnel experiment

To demonstrate that the new airfoil exhibit higher aerodynamic performance, wind tunnel experiments for the WT180 airfoil were carried out for both smooth and rough conditions in a 3.0 × 1.6 m low-speed wind tunnel, and three Reynolds number values (2.0×10^6, 3.0×10^6, and 4.0×10^6) were chosen during the tests. The Mach number is 0.1, 0.16 and 0.22, respectively. The test stand shown in Fig. 7 was built for 2D airfoil testing.

4.1. Instrumentation

To measure the static and total pressure, pitot tubes were installed at different locations in the test section. This effort was to determine the wind tunnel reference pressures and estimate the turbulence level. The airfoil was equipped with 92 pressure

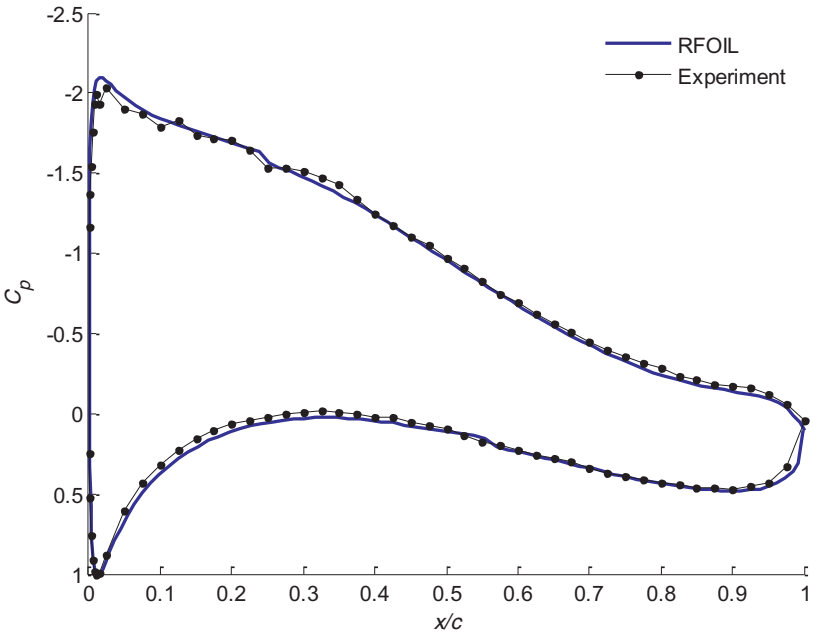

Fig. 9. Comparison of the measured and RFOIL predicted pressure coefficient distribution at the max-lift/drag ratio.

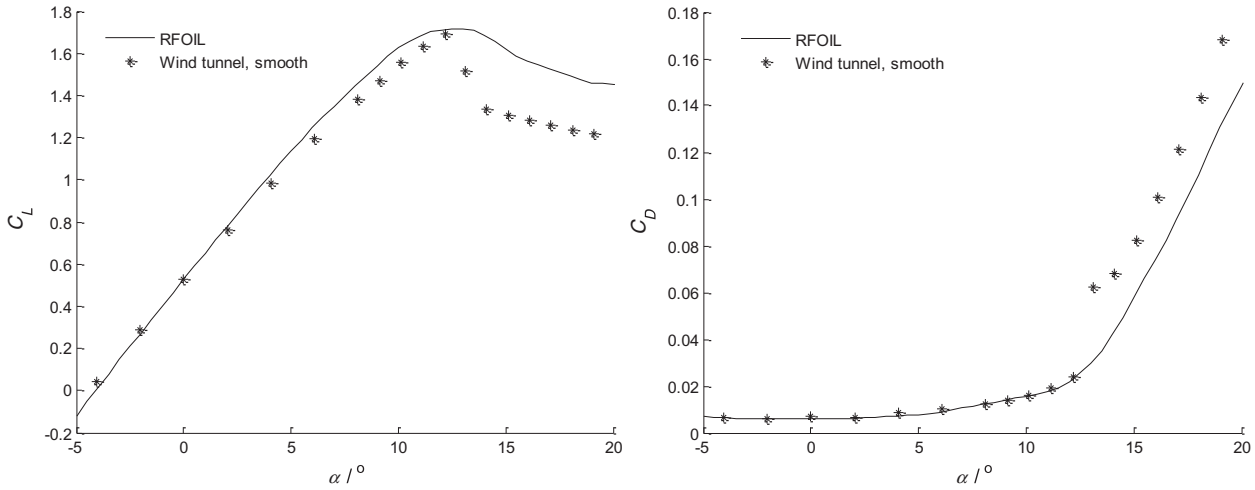

(a) Lift coefficient (b) Drag coefficient

Fig. 10. The WT180 predicted (RFOIL) and measured lift coefficient and drag coefficient for smooth surface flow at Re = 3.0×10^6.

taps, all of which were placed along the chord at the centre line of the model in a staggered alignment, so that disturbance from upstream taps can be minimised. The pressure taps were carefully distributed in a manner through which the expected pressure gradients can be adequately resolved. It should be noted that on the upper and lower surfaces, the tap spacing was dense in 5% of the leading edge region.

The wake rake was equipped with as many as 187 total pressure tubes and 9 static pressure tubes, respectively. The wake rake was fixed 1.3 airfoil chords (1.04 m) away from the airfoil trailing edge, with its centre approximated to the height of the trailing edge with zero incident angles and behind the centre line of the airfoil section.

4.2. Leading edge roughness

Leading edge roughness was measured out of the necessity to simulate the influence of accumulated dirt and bugs on the wind turbine airfoil. It was determined with 3 mm wide orthogonal zigzag tape with a thickness of 0.35 mm, which is placed 5% chord on both the airfoil suction side and the pressure side.

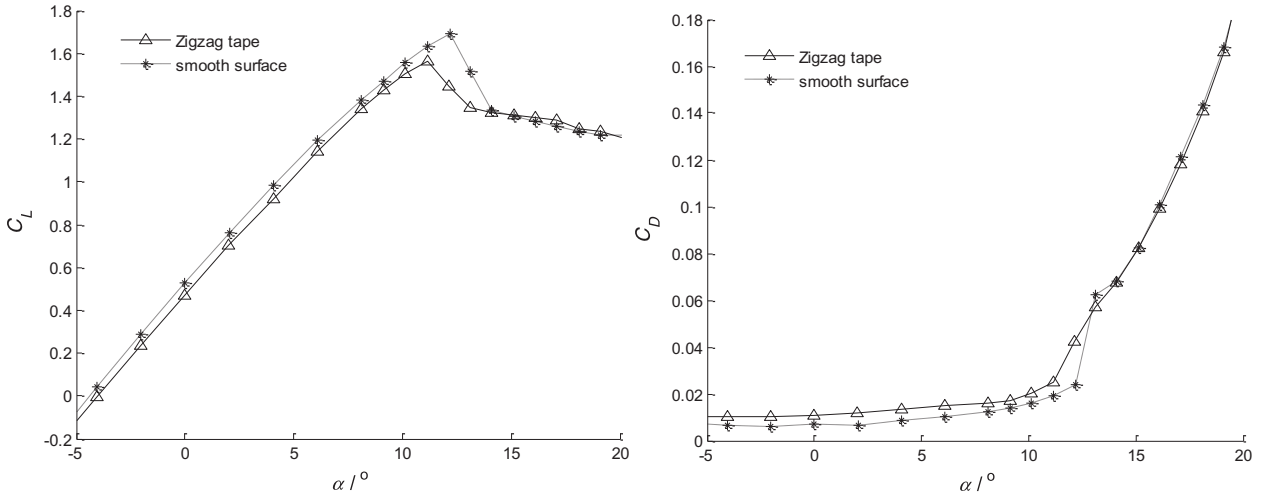

Fig. 11. The WT180 measured lift coefficient and drag coefficient with leading edge roughness compared with smooth surface flow at Re = 3.0 × 10^6.

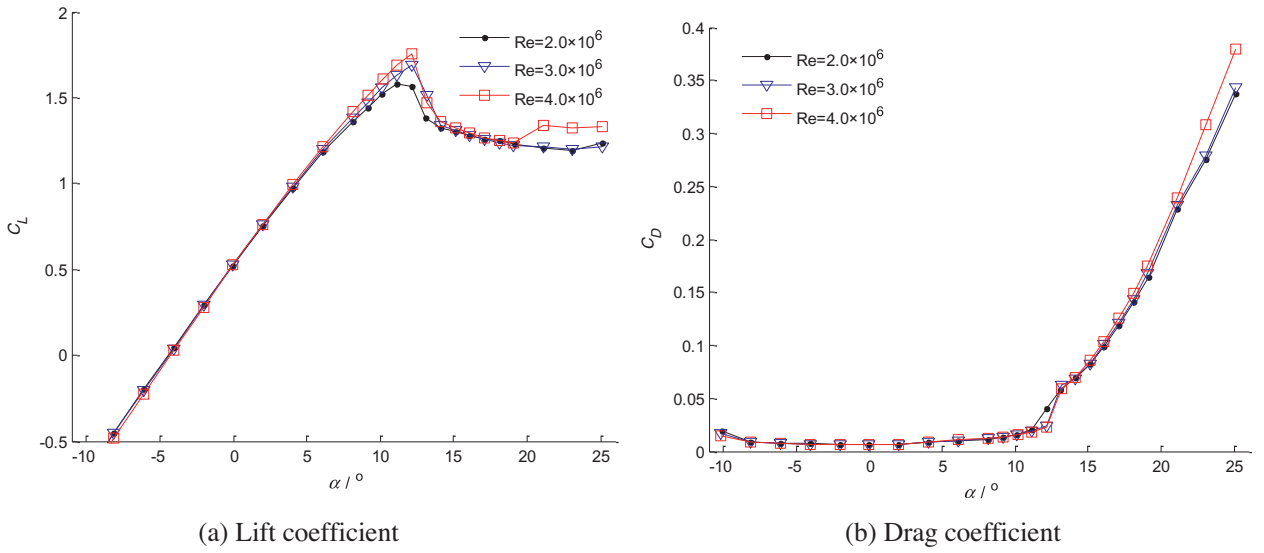

Fig. 12. Variation in the lift and drag with Reynolds number for the smooth configuration.

4.3. Testing results

Fig. 8 shows the measured pressure distributions for smooth surface flow at Re = 3.0 × 10^6. The pressure distributions at the angle of attack of the minimum drag, maximum lift/drag ratio and maximum lift coefficient are illustrated in the figure. Fig. 9 shows the WT180 measured and RFOIL predicted pressure distributions at the angle of attack of the maximum lift/drag ratio. The measurement and the numerical prediction showed desirable agreement. The suction side pressure distribution of this airfoil showed a significant peak at the leading edge, which facilitates the pressure recovery towards the trailing edge and, meanwhile, secures the airfoil against separation. Despite some loading was distributed over the trailing edge, most of the loading was distributed over the leading edge.

Fig. 10 shows the measured C_L and C_D of the WT180 airfoil for smooth flow (free transition) compared with numerical prediction. The difference of the maximum C_L between the measured value (1.6902) and the predicted value (1.717) is within 2% for smooth flow. The shape of C_L versus α was linear until just before C_{Lmax}, the stall was well defined and the post-stall region was smooth. The minimum C_D was measured as 0.0059 in agreement with the predicted value of 0.00592. The value of the measured lift and drag coefficients are different for the calculation in the post-stall region. The reason is that it is hard to predict accurately the aerodynamic performance using the flow solver RFOIL in deep stall.

Fig. 11 shows the measured C_L and C_D comparison with the cases of leading edge roughness (0.35 mm zigzag tape) and a smooth surface condition. The sensitivity of the airfoil to leading edge roughness is a little high, as can be deduced from Fig. 11, in which the effect of zigzag tape is shown. It can be observed that leading edge roughness does not affect the slope of C_L versus α, but it causes a drop in C_{Lmax} of 7.7% to 1.56. Leading edge roughness also causes an increase in the minimum C_D and thereby reduces the C_L/C_D ratio. The reason is that the high lift coefficient in free transition is pursued. However, the high lift coefficient in smooth condition is contradictory with low roughness sensitivity.

Fig. 12 shows the measured aerodynamic forces of the WT180 airfoil for three Reynolds numbers in the approximate range of 2.0×10^6 –4.0×10^6. The results demonstrate that $C_{L\text{-}max}$ changes slightly with Reynolds number (from 1.5813 at Re $= 2.0\times10^6$ to 1.7562 at Re $= 4.0\times10^6$), and the stalling angle remains approximately 11°.

5. Conclusion

Based on Taylor high-order polynomial series, a novel parametric representation method of the "Shape function" for airfoils was developed. The design space and shape control function of the airfoil have been studied in detail. The optimised mathematical model of the airfoils is established combing GA method and the flow solver RFOIL. WT airfoil series were designed by optimising the coefficients of the shape function for airfoils. Compared with some commonly used wind turbine airfoils, the new airfoils showed better on-design and off-design aerodynamic performances.

Wind tunnel experiments for WT180 were carried out for both clean and rough surface conditions in the 3.0 × 1.6 m low-speed wind tunnel, and three Reynolds numbers were chosen during the tests. The test verified the high lift/drag ratio and the high maximum lift coefficient for the WT180, but the airfoil was found to be a little sensitive to leading edge roughness. Therefore, some new airfoils with high aerodynamic performance and low roughness sensitivity will be designed in the future work. Comparisons of the RFOIL prediction and experimental results generally show good agreement. The novel design theory and methodology for wind turbine airfoil proposed in this paper is verified by the wind tunnel experiments. This approach has great significance for the development of new blades.

Acknowledgements

This work is supported by a grant from the National High Technology Research and Development program of China (863 Program, no. 2012AA051301) and National Natural Science Foundation of China (no. 51175526, no. 51405140).

References

[1] Tangle J L, Somers D M. NREL airfoil families for HAWTs. WINDPOWER'95, Washington D.C. Proc. 1995, 117-123
[2] Eppler, Richard: Airfoil Program System "PROFIL00." User's Guide. Richard Eppler, 2000.
[3] J.L. Tangler, D.M. Somers, Status of the Special Purpose Airfoil Famolies, in: Proceedings of WINDPOWER'87, San Fransisco, U.S.A, 1987, pp. 229–335.
[4] van Rooij, R.P.J.O.M., Modification of the boundary layer calculation in rfoil for improved airfoil stall prediction, Report IW-96087R, TU-Delft, the Netherlands.
[5] R.P.J.O.M. van Rooij, W.A. Timmer, Roughness sensitivity considerations for thick rotor blade airfoils, J. Solar Energy Eng 125 (2003) 468–478.
[6] WA Timmer, P.R.J.O.M. van Tooij, Summary of the Delft University wind turbine dedicated airfoils, J. Solar Energy Eng 125 (2003) 488–496.
[7] P. Fuglsong, C. Bak, Development of the risø wind turbine airfoils, Wind Ener 7 (2004) 145–162.
[8] P. Fuglsong, K.S Dahl, Design of the new risø-al airfoil family for wind turbines, in: European Wind Energy Conference, Vol. 1-5, Nice, France, 1999, pp. 134–137.
[9] M. Drela, XFOIL: an analysis and design system for low Reynolds number airfoils, in: Low Reynolds number Airfoil Aerodynamics; Proceedings of the Conference, June 5-7, 1989, University of Notre Dame, Germany, 1989, pp. 1–12.
[10] H. Sobieczky, Parametric airfoils and wings, Notes Numer. Fluid Mech 68 (1998) 71–88.
[11] J. Hájek, Parameterization of airfoils and its application in aerodynamic optimization, in: Proceedings of the 16th Annual Conference of Doctoral Students - WDS 2007. WDS'07 Proceedings of Contributed Papers part1, June 5-8, 2007, Charles University, Prague. Czech republic: Matfyzpress, 2007, pp. 233–240.
[12] A. Bjork, Coordinates and Calculations for the FFA-W1-xxx, FFA-W2-xxx and FFA-w3-xxx series of Airfoils for horizontal axis wind turbines, FFA TN, Stockholm, Sweden, 1990.
[13] B.I. Soemarwoto, T.H.E. Labrujere, Airfoil design and optimization methods: recent progress at NLR, Int. J. Numer. Meth. Fluids 30 (1999) 217–228.
[14] S.M. Habali, I.A. Saleh, Design and testing of small mixed airfoil wind turbine blades, Renewable Ener 6 (2) (1995) 161–169.
[15] J.W. Larsen, S.R.K. Nielsen, S. Krenk, Dynamic stall model for wind turbine airfoils, J. Fluids Struct 23 (2007) 959–982.
[16] J.P. Baker, E.A. Mayda, C.P. van Dam, Experimental analysis of thick blunt trailing-edge wind turbine airfoils, J. Solar Ener. Eng 128 (11) (2006) 422–431.
[17] L. Bermudez, A. Velazquez, A. Matesanz, Viscous–inviscid method for the simulation of turbulent unsteady wind turbine airfoil flow, J. Wind Eng. Ind. Aerodyn 90 (2002) 643–661.
[18] A.F.P. Ribeiro, A.M. Awruch, H.M. Gomes, An airfoil optimization technique for wind turbines, Appl. Math. Model 36 (2012) 4898–4907.
[19] Shen WZ, Chen J., Cheng J.T. et al. Airfoils and methods for designing airfoils. Application No. PCT/EP2010/056810, International patent application.
[20] IraH. Abbott, AlbertE. Von Doenhoff, Theory of wing sections [M], Dover Publications, INC, New York, 1959.